



3D FE adhesion failure analyses of adhesive bonded single lap joint made with functionally modulus graded curved adherends

S. K. Parida¹ · A. M. Murmu¹ · Vemireddy Hari² · Vivek S. Ayar³ · Ratnakar Das¹

Received: 24 April 2024 / Accepted: 29 June 2024

© The Author(s), under exclusive licence to Springer-Verlag France SAS, part of Springer Nature 2024

Abstract

Adhesive bonded Single Lap joints (SLJ) are used to make several larger structures of several industries, including (aerospace and marine) by joining smaller laminated FRP composite panels. The Single Lap Joint, due to its inherent overlapping geometry, possesses an eccentric load transfer path when subjected to tensile loading. The coupling of differential straining, bending, twisting and tension phenomenon induces out-of-plane peel, in-plane longitudinal shear and transverse shear stresses near the overlap ends. A small adhesion failure may be pre-existing or may onset from a vulnerable location in the Single Lap Joint. The propagation rate of this adhesion failure decides whether the jointed structure will fail slowly or catastrophically during loading. A three-dimensional adhesion failure analysis in the Single Lap Joint made with functionally modulus-graded curved adherends under uniformly applied tension is presented in this article. The peel and shear stresses in the bond line interfaces have been evaluated for different compositional gradient exponents of the material of adherends using the non-linear finite element method. The effects of the adhesion failure lengths and compositional gradient exponents on the opening, sliding and strain energy release rate (SERR) corresponding to have been evaluated to predict the structural integrity of the SLJ. The structural integrity and, hence, the service life of the adhesive-bonded single lap joint can be enhanced by the functionally graded modulus of the adherends to reduce the magnitudes of peel and shear stresses in the vicinity of the overlap ends.

Highlights

- Simulation of adhesion failure growth.
- The structural integrity of the jointed structure made with curved panels has been assessed.
- Use of functionally modulus grading scheme to slow down the crack growth.

Keywords Functionally graded material (FGM) · Single lap joint (SLJ) · Adhesion failure · Strain energy release rate (SERR) · Virtual crack closure technique (VCCT)

✉ A. M. Murmu
anand.murmu@gmail.com

S. K. Parida
skparida@niamt.ac.in

Vemireddy Hari
hari@iitbbs.ac.in

Vivek S. Ayar
vsayar@niamt.ac.in

Ratnakar Das
ratnakardas@niamt.ac.in

¹ Department of Mechanical and Manufacturing, National Institute of Advanced Manufacturing Technology Ranchi, Ranchi 834003, Jharkhand, India

² School of Mechanical Engineering, Indian Institute of Technology, Bhubaneswar Samantapuri, 751013 Bhubaneswar, Odisha, India

³ Department of Foundry and Forge Technology, National Institute of Advanced Manufacturing Technology, Ranchi 834003, Jharkhand, India

1 Introduction

Adhesive bonded single lap joints (SLJ) join flat or curved panels in several industries. The use of adhesive joints has an inherent advantage of reduced stress concentration compared to bolted and riveted joints. The significant factors causing the adhesion failure in the adhesive-bonded SLJ are the high gradients of stresses at the overlap ends. Hence, using the functional modulus graded adherends in SLJ with Young's modulus gradually varying along the length of the adherends in the overlapping region and outside of is a potential way to reduce the stress peaks at the overlap ends. Further, the pre-existing adhesion failure, if any, near the joint's vulnerable (overlap ends) region and its propagation gradually reduces the strength and stiffness, so it is an important design criterion. This research employed finite element analyses to analyse the effect of different material grading schemes to achieve stress distribution to improve structural integrity by reducing the rate of adhesion failure propagation.

Some important lap joint theories developed are by Volkersen [1], Banea and da Silva [2], Wang and Yau [3], and Tong [4]. Volkersen [1] analysed a single lap joint under extension, ignoring the effect of tearing stress at the end. Tay's [5] paper overviews developments from 1990 to 2001. The various research works on lap shear joints include that of Wang and Yau [3], Carpenter [6], Wang and Raju [7], Tong [4], Cheuk and Tong [8], Edde and Verreman [9], and Lai et al. [10], etc. Most of the reports are based either on simplified analytical formulations or experiments—some of the work involved employed finite element procedures. But most of them were two-dimensional. So far, the three-dimensional FE analyses lack newer modelling methods with contact and Multi-Point Constraint (MPC) elements.

Apalak [11] investigated the variation of stress states of adhesively bonded tubular single lap joints made with functionally graded material subjected to thermo mechanical loading. Young's modulus of the tubular adherends is graded along the thickness. The elastic and thermos-residual stress analysis was carried out for a uniform temperature drop using an isoperimetric layered finite element where the material properties differ in different layers. S Kumar [12] presented an analytical procedure for tubular SLJ using adhesive whose properties are graded along the radial direction, simplifying assumptions of no variation of shear stress along the thickness of the adhesive. Reddy [13] investigated through-the-thickness stress variations in a functionally graded plate using the third-order shear deformation plate theory considering the thermomechanical coupling, dependency on time and the von Karman-type geometrical non-linearity. Cengiz and Mehmet [14] carried out a two-dimensional phase-field finite element analysis of SLJ made

with flat adherends using functionally graded adhesive and cohesive zone modelling and reported that functional grading of materials of the adhesive and overlap length could be a possible way to prevent delamination in the adherends. Mehdi et al. [15] reported that functionally graded adhesive in stepped single-lap joints can improve joint strength. His model considered the fractional Zener model to input visco elastic properties of the adhesive and the bending moment arising due to an eccentric loading path. Khan et al. [16] investigated the variation of the failure prompting stress in the adhesive due to random variation of the adhesive's material properties using a linear elastic model in a double lap joint. They proposed a stiffer adhesive with a longer overlap length, which was better. A mixed mode failure, i.e., the cohesive failure in the adhesive and delamination failure between the layers of fibre-matrix in composite adherends of SLJ, has been investigated using 3-D FE and hybrid adhesive by Kim et al. [17].

However, no literature dealing with the prediction of adhesion failure propagation in single lap joints made with curved adherends has been reported, and the effect of functionally modulus-graded material on the rate of adhesion failure propagation has been reported till now. The critical application areas of adhesive-bonded SLJs in the aircraft and chemical industries usually involve joining curved panels. From the literature review, it is inferred that by employing a suitable functional grading scheme in the design of the SLJ, one can effectively reduce the stress concentration, rate of propagation of the adhesion failure and delaminations and hence the overall performance of the SLJ. The research gap is to find a suitable functional grading scheme of the adherends material so that the growth and propagation of pre-existing adhesion failure can be slowed down or prevented. Accordingly,

The present research is aimed at analysing the SLJ with the following objective:

- (i) The effects variation of the compositional gradient (n) of the materials of the adherends on the stresses ($\sigma_r, \tau_{rz}, \tau_{r,\theta}$) in the interface of adhesive and adherends.
- (ii) Analyses of SLJs of the curved panels made with FGM taking curvature effects into account.
- (iii) SERR variations for varying lengths of adhesion failure in an SLJ made with FGM curved panels of different compositional gradient exponent.
- (iv) Effect of adhesion failure sizes on the SERR.
- (v) Suitable design recommendations for SLJ of curved panels using FGM adherend.

Fig. 1 Adhesive bonded SLJ of curved panels made with functionally modulus graded materials having the angle of arc $\theta = 20^\circ$

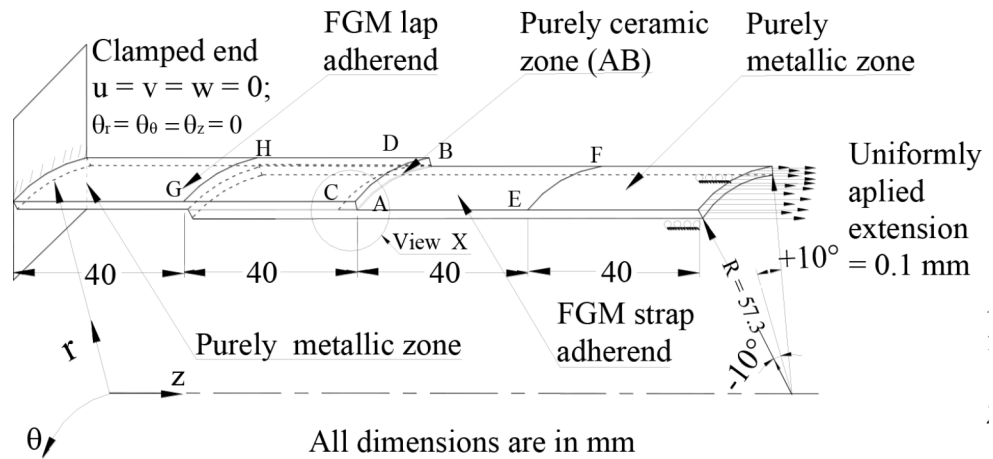


Table 1 Mechanical properties of constituents of the FGM curved adherends

Material Properties	Constituents of FGM adherends material		Epoxy adhesive
	Ceramic(Al_2O_3)	Metal (Ni)	
Young's Modulus	$E_c = 393GPa$	$E_m = 199.5GPa$	$E_a = 2.8GPa$
Poisson's Ratio	$\nu_c = 0.25$	$\nu_m = 0.3$	$\nu_a = 0.4$

1.1 The schematic representation of the SLJ

In this research, the three-dimensional non-linear finite element analyses of the SLJ made with curved functionally graded adherends are carried out. The lap and strap adherends are joined by isotropic adhesive, as shown in Fig. 1.

Figure 1 shows the schematic of the SLJ made with 20° curved panels. The thickness of the lap and strap adherends is 2 mm , and that of adhesive is $t_a = 0.2\text{ mm}$. The inner radius of the strap adherend is $R = 57.3\text{ mm}$. Five different circumferentially curved adhesion failure lengths of magnitudes $a = 2, 4, 6, 8\text{ mm}$ and 10 mm have been taken to simulate the growth of adhesion failure. One end of the SLJ is clamped, and the other end is loaded with uniform applied strain $\epsilon = 0.1\text{ mm}$, as shown in Fig. 1. The curved panel geometry in the present analysis is considered to have the angle of the arc of the curved panel $\theta = 20^\circ$ such that the arc length of the inside of the strap adherend is equal to 20 mm . Parametric studies have also been carried out for different angles of the panel's arcs (shallowness angle $\theta = 20^\circ, 25^\circ, 30^\circ$). The radius of curvature of various panels is chosen such that the inside arc length of the strap adherend = 20 mm to evaluate the effect of curvature geometry on stresses ($\sigma_r, \tau_{rz}, \tau_{r\theta}$). The material properties of the constituent material of FGM are given in Table 1.

1.2 Schematic representation of the functionally graded materials of the adherends

The adherends are made from a mixture of ceramic (Al_2O_3) and metal (Ni). The material properties gradation of adherends can be obtained by continuously varying its

constituents, shape and size of the particles and their volume fraction as suggested by Koizumi [18]. The variations in material properties along the axial direction of the curved lap and strap adherends are shown in Fig. 2(a) and (b) as per the power law given in Eqs. 1–4.

$$E_{cm}(Z) = E_m + (E_c - E_m)\left(\frac{c}{M}\right)^n \quad (1)$$

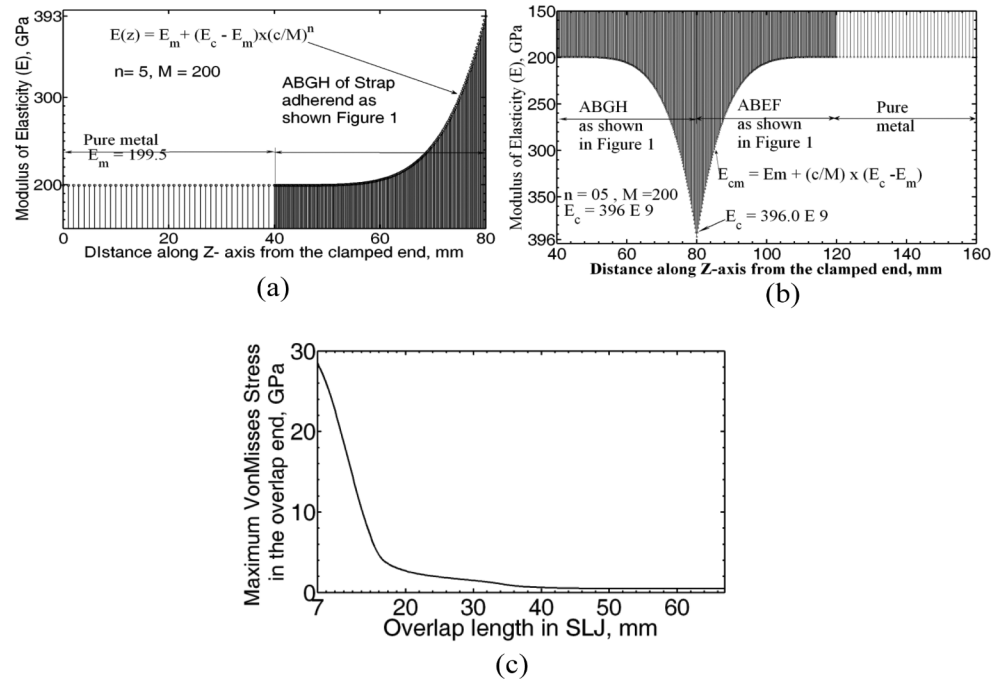
$$\nu_{cm}(z) = \nu_m + (\nu_c - \nu_m)\left(\frac{c}{M}\right)^n \quad (2)$$

$$E_{cm}(Z) = E_c - (E_c - E_m)\left(\frac{c}{M}\right)^n \quad (3)$$

$$\nu_{cm}(z) = \nu_c - (\nu_c - \nu_m)\left(\frac{c}{M}\right)^n \quad (4)$$

where, E_c, E_m and ν_c, ν_m are Young's moduli of elasticity and Poisson's ratios for purely ceramic and purely metallic materials, respectively. E_{cm}, ν_{cm} Young's modulus of elasticity and Poisson's ratio of material having partly metallic and partly ceramics, respectively. The symbols n, c, M are the compositional gradient exponent, the number of layers and the maximum number of elements. The variation of modulus of elasticity (E) of adherend materials having different compositional gradient exponent (n) along the z-axis is shown in Fig. 2(a) & (b) for a typical value of $n = 5$. The material properties of constituents of FGM adherend and the adhesive are listed in Table 1. The material properties are adopted from the paper by APALAK.

Fig. 2 (a) Modulus of Elasticity gradation along the lap adherend along the z-axis. (b) Modulus of Elasticity gradations along the strap adherend along the z-axis. (c) Variations maximum value of von Mises stress at overlap end of SLJ of curved adherend made with FGM material of $M=200$, $n=10$ for $\theta = 20^\circ$



As a characterising parameter in adhesion failure propagation, the strain energy release rates are evaluated from 3-D FE analysis using the virtual crack closure technique proposed by Rybiki and Kanninen [19], Behera et al. [20]. The details of the evaluation of SERR are presented in Sect. 3.

1.3 Computational procedure and FE modelling of adhesion failure analysis in SLJ made with curved functionally graded adherends

An initial investigation has been carried out to determine the optimum overlap length of the SLJ, based on maximum values of von Mises stress at the overlap end for different overlap lengths from 7 to 65 mm, which are plotted in Fig. 2 (c).

The magnitude of von Mises stress sharply decreases with the increase in the overlap length of the lap and strap of the SLJ. However, there is no appreciable decrease in the magnitude of von Mises stress for overlap lengths beyond 35 mm. Hence, the optimum overlap length is 40 mm throughout the analyses.

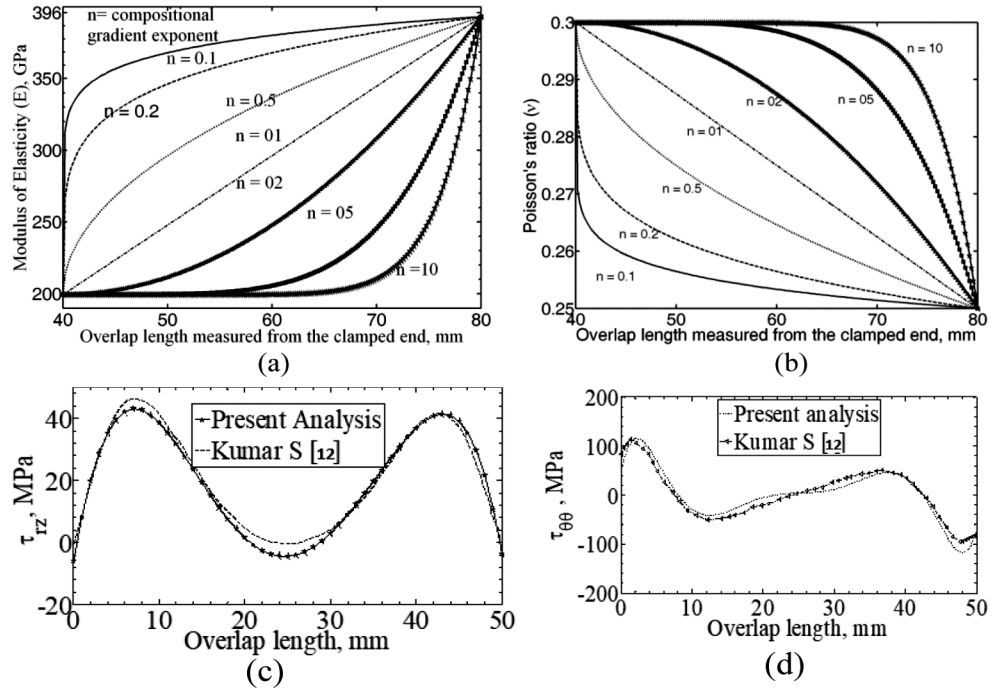
ANSYS Parametric Design Language (APDL) code of the FE software ANSYS 13.0 is used to model the SLJ. The adherends and the adhesive are modelled using 8 noded isoperimetric brick elements (SOLID 185). The variations of modulus of elasticity (E) and Poisson's ratio (ν) along the z-axis of the adherend materials are input by writing APDL code as per power law given below (Eqs. 1, 2, 3 and 4). The plot of the power law variations modulus of elasticity (E) along the z-axis in the overlapped region is given in Fig. 2(a) & (b). The functional variation of adherends'

materials with different composition gradients, which are input to the ANSYS software, are represented in Fig. 3(a) & (b).

The number of finite elements used to mesh the FGM adherends in the overlapped region along the z-axis is called layer number (M) Apalak et al. [11]. The mechanical properties are varied from purely metallic to purely ceramic. It is observed from several analyses that mesh convergence is achieved by taking a number of elements $M=200$ in the overlap region. The eight noded isoparametric brick elements have also been used to model the adhesive layer. At failure interfaces, duplicate nodes have been defined between the adhesive and the adherends. In the uncracked region, the corresponding nodes of the adherend and the adhesive merge so that continuity conditions prevail. By sequentially unmerging these nodes at the adherend adhesive interface, gradual propagation of the adhesion failure can be simulated. Contact elements connect the co-existing nodes in the adhesion failure region to stop the inter-penetration of the adhesive and adherend during loading.

Adhesion failure analysis using the energy release rate (SERR) criterion is considered to be a very useful parameter for predicting the damage growth Behera et al. [20]. The detailed SERR computation procedure is described in research by Pradhan and Parida [21].

Fig. 3 (a) Variations of modulus of elasticity (E) along the overlap length adherends along the z-axis for different values of compositional exponent gradient (n). Values of compositional exponent gradient (n). (b) Variations of Poisson's ratio (ν) along the overlap length adherends along the z-axis for different values of compositional exponent gradient (n). (c) Comparison of shear stress (τ_{rz}) with the results obtained by Kumar S [12]. (d) Comparison of shear stress ($\sigma_{\theta\theta}$) with the results obtained by Kumar S [12]



2 Computation of SERR in cylindrical (r, theta and z) coordinate system

2.1 Method of computation by modified crack closure integral (MCCI)

In the MCCI method of computation, the SERRs of the opening, shearing and transverse shearing modes of failure G_I , G_{II} and G_{III} are computed as follows:

$$G_I = \lim_{\Delta A \rightarrow 0} \frac{1}{2\Delta A} \int_a^{a+\Delta a} \int_{-\frac{r\Delta\theta}{2}}^{\frac{r\Delta\theta}{2}} \sigma_r(\theta, z) \times [u_{top}(\theta, (z - \Delta a)) - u_{bottom}(\theta, (z - \Delta a))] r d\theta dz \quad (5)$$

$$G_{II} = \lim_{\Delta A \rightarrow 0} \frac{1}{2\Delta A} \int_a^{a+\Delta a} \int_{-\frac{r\Delta\theta}{2}}^{\frac{r\Delta\theta}{2}} \tau_{rz}(\theta, z) \times [w_{top}(\theta, (z - \Delta a)) - w_{bottom}(\theta, (z - \Delta a))] r d\theta dz \quad (6)$$

$$G_{III} = \lim_{\Delta A \rightarrow 0} \frac{1}{2\Delta A} \int_a^{a+\Delta a} \int_{-\frac{r\Delta\theta}{2}}^{\frac{r\Delta\theta}{2}} \tau_{r\theta}(\theta, z) \times [v_{top}(\theta, (z - \Delta a)) - v_{bottom}(\theta, (z - \Delta a))] r d\theta dz \quad (7)$$

Subscripts top and bottom correspond to the top and bottom surfaces in the adhesion failure region, respectively, as shown in Figure. The adhesion failure length is denoted by l_{af} and $l_{\Delta af}$ is the virtual adhesion failure length caused due to the external loading. Here, $[u_{top}, v_{top}, w_{top}]$ are the displacements of the top layer, and $[u_{bottom}, v_{bottom}, w_{bottom}]$ corresponds to that of nodes of the bottom surfaces in the adhesion failure, respectively, behind the adhesion

failure front, and $\sigma_r(\theta, z), \tau_{rz}(\theta, z), \tau_{r\theta}(\theta, z)$ are the nodal stresses in the adhesion failure front required to close the already failed surfaces. The area $\Delta A = (\Delta a \times r\Delta\theta)$ is considered to be closed to compute the components of SERR using the MCCI method.

2.2 Computation method of SERR using virtual crack closure technique (VCCT) in cylindrical (r, theta and z) coordinate system

In the Rybicki and Kanninen [14] Method of computing SERR using VCCT, the equations (5 to 7) take the form of equations (5 to 7) if the following conditions are taken care of during FE modelling. The FE meshing pattern should be symmetric in the plane of crack propagation, (ii) the element size should be taken after mesh convergence studied, and (iii) the normal of each element across the failure plane in the FE mesh should face each other. In the VCCT method, the SERR of individual modes can be obtained by multiplying corresponding nodal forces at the FE nodes ahead of the adhesion failure front and nodal displacements behind it. As per the VCCT procedure, the components of SERR for the SLJ with curved panels and containing adhesion failure are calculated as follows:

$$G_I = \frac{1}{2\Delta A} R_f (u_{top} - u_{bottom}) \quad (8)$$

$$G_{II} = \frac{1}{2\Delta A} Z_f (w_{top} - w_{bottom}) \quad (9)$$

$$G_{III} = \frac{1}{2\Delta A} \theta_f (v_{top} - v_{bottom}) \quad (10)$$

The virtual elemental area $\Delta A = (\Delta a \times r \Delta \theta)$ must be virtually closed during SERR computation, and the nodal forces $R_f, Z_f \theta_f$ correspond to the opening, sliding and tearing forces needed to prevent adhesion failure propagation growth. Here, $[u_{top}, v_{top}, w_{top}]$ and $[u_{bottom}, v_{bottom}, w_{bottom}]$ have the same meaning as in Eqs. 5–7.

2.3 Validation of the present FEA method with the results of Kumar [12]

The adhesive is generally exhibits lower strength than adherends. Hence, the stress distributions in the adhesive region are important in failure analysis. To validate the present FE method, stresses (τ_{rz} and $\tau_{\theta\theta}$) in the mid-layer of the adhesive are evaluated for a problem reported by Kumar [12] maintaining the same geometry, loading and boundary conditions using the present FE procedure. Scientifically graded mesh with higher mesh density at the overlap end of the joint was taken as per the procedure described by Behera et al. [20]. The stresses (τ_{rz} and $\tau_{\theta\theta}$) in the mid-plane of the functionally graded adhesive is plotted to validate the present FE analysis method against the results available in the literature by Kumar [12]. Results (Fig. 3 (c) and (d)) from the present FE analysis, which used 8 noded isoparametric elements (Solid 185) with functionally modulus graded material properties of adhesive for tubular adhesive joints of the same geometry and loading were compared with the results obtained in the analysis by Kumar S [12]. The stresses $\tau_{rz}, \sigma_{\theta\theta}$ obtained by the present study are in close agreement.

3 Results and discussion

3.1 Effect of the compositional gradient (n) in adherends on peel and shear stress distributions in the adhesive-adherend interface of the SLJ made with a curved panel along the z-axis

This section discusses the effects of the materials grading scheme on the adherends of the SLJ to reduce the growth of pre-existing adhesion failure. The impact of the curvature of the adherend at vulnerable locations has been carried out by three-dimensional finite element analyses of the SLJ containing a pre-existing adhesion failure. The propagation rate of pre-existing adhesion failure has been quantified for several functional grading schemes by computing the strain energy release rates in the vicinity of the adhesion failure fronts.

The variation of material properties for different compositional gradients can be referred to in Fig. 3 (a) and (b). Figure 4(a) to (i) show the peel and shear stress distributions for varying compositional gradient exponent (n) in the overlapped region at the interface of the adhesive and lap adherend at $R=59.3$ mm, which happens to be the critical location. The peel and shear stress peaks at the overlap end at 40 mm and 80 mm from the overlap ends. The peel stress is maximum at 80 mm from the clamped end for $n=0.1$. It is higher in the central region than at the edges. The peel stress magnitude decreases from 87 MPa for $n=0.1$ to 60.5 MPa for $n=10$. However, for an increase in the value of the compositional gradient exponent from $n=5$ to $n=10$, the magnitude of the peel stress does not decrease much. Shear stress (τ_{rz}) also decreases for higher compositional gradients. Thus, the compositional gradient $n=5$ is a good enough value to have minimum peel and shear stress.

3.2 Effect of curvature of adherends on stress distributions in the interface of adhesive-adherend of the SLJ

Results of parametric studies for different geometries of the curved panel in SLJ are presented in Fig. 5 (a) to (f). The radius and the angle of the arc of the curved adherends vary so that the width of the panel is the same for different analyses. The loading and the boundary conditions are kept the same for all the geometry considered in the study to see the effect of the curvature of adherent on peel stress distributions in the bond line interface of the SLJ. Figure 5(a) shows that both peel and shear stresses are more in the adhesive-lap interface than the adhesive-strap interface in the clamped side, whereas peel stress (σ_r) is more in the adhesive-strap interface ($R=59.3$ mm) and magnitude of shear stress (τ_{rz}) is more in the adhesive-lap interface ($R=59.5$ mm) at the overlap end on the loading side (Fig. 5 (b)). Similar observations are obtained when the shallowness angle (θ) is increased to 25° (Fig. 5(c-d)) and $\theta = 30^\circ$ (Fig. 5(e-f)). From Fig. 5 (a) to (f), it is evident that the peak values of both stresses (σ_r, τ_{rz}) decrease marginally. The locations of the peak values of stresses (σ_r, τ_{rz}) follow the same pattern.

3.3 SERR variations for varying adhesion failure lengths in an SLJ made with FGM curved panels having different compositional gradient exponent

Figure 6 Variations of SERR with adhesion failure sizes along the circumferential width $\theta = 20^\circ, M = 200, n = 0.1$.

Strain Energy Release Rate is an indicative parameter for the assessment of growth of adhesion failure, as suggested by Behera et al. [20]. Accordingly, MCCI *vis-à-vis* VCCT

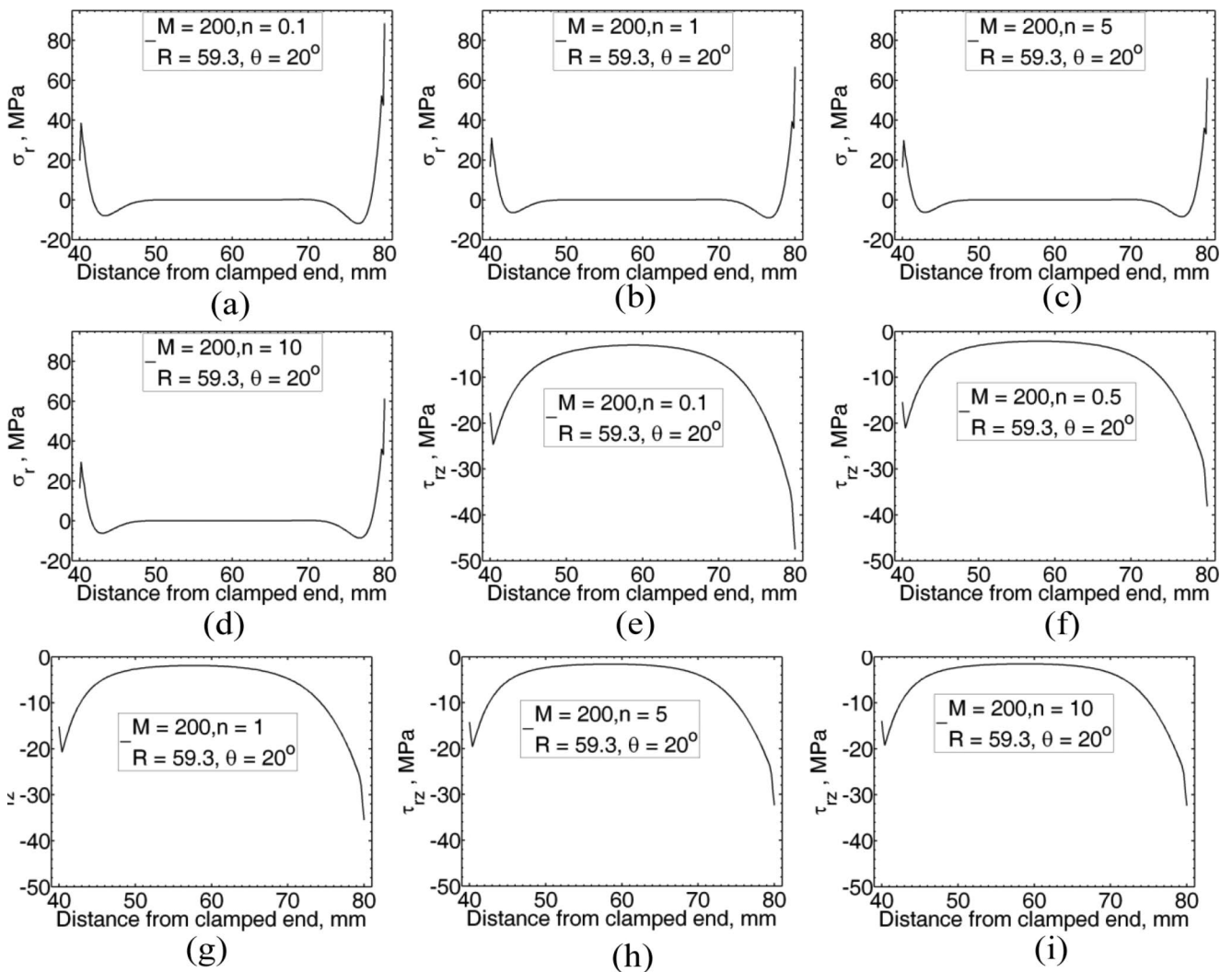


Fig. 4 Variation of the peel and shear stress distributions for varying compositional gradient exponent (n) in the overlapped region. (a) Peel stress for $n = 0.1$. (b) Peel stress for $n = 1$. (c) Peel stress for $n = 05$. (d) Peel stress for $n = 10$. (e) Shear stress for $n = 0.1$. (f) Shear stress for $n = 0.5$. (g) Shear stress for $n = 1$. (h) Shear stress for $n = 5$. (i) Shear stress for $n = 10$

has been used to compute G_I, G_{II} , and G_{III} for opening, sliding and cross-sliding modes of adhesion failure propagation, respectively, along the adhesion failure fronts of varying sizes to simulate the adhesion failure growth rate. The SERR values are calculated for adherend’s material with different functional grading schemes and plotted in Fig. 6(a-c). The inter-laminar stresses ($\sigma_r, \tau_{rz}, \tau_{r\theta}$) have been used to evaluate G_I, G_{II} and G_{III} in the MCCI computation method by using equations (5 to 7). The VCCT methods are straightforward and convenient for computations. This is indicated in Sect. 3.2. Hence, Equations (8 to 10) have been used for the above computations. It has been seen that both of them have yielded the same results as per observation made by Rybicki and Kanninien [14].

The following observations are made regarding the variations of individual components of SERR:

- (i) The magnitude G_{II} is larger than G_I . The value G_{II} increases as adhesion failure propagates. (Fig. 6(b)). Both G_I and G_{II} decrease for higher values of the compositional gradient.
- (ii) The G_{II} values vary along the circumferential width of the adhesion failure front, having a maximum in the central region and a minimum at the free edges (Fig. 7(a)). The G_I variations show a trend reverse to those of G_{II} (Fig. 7(b)). The magnitude of G_{III} values is comparatively much lower than those of G_I and G_{II} .

The value ($G_T = G_I + G_{II} + G_{III}$) decreases with the increase of the compositional gradient, as shown in Fig. 6(c). The $G_T n = 10$ has a minimum value for overall crack sizes. However, the decrease in the magnitude of SERR for $n = 5$ to $n = 10$ is not much.

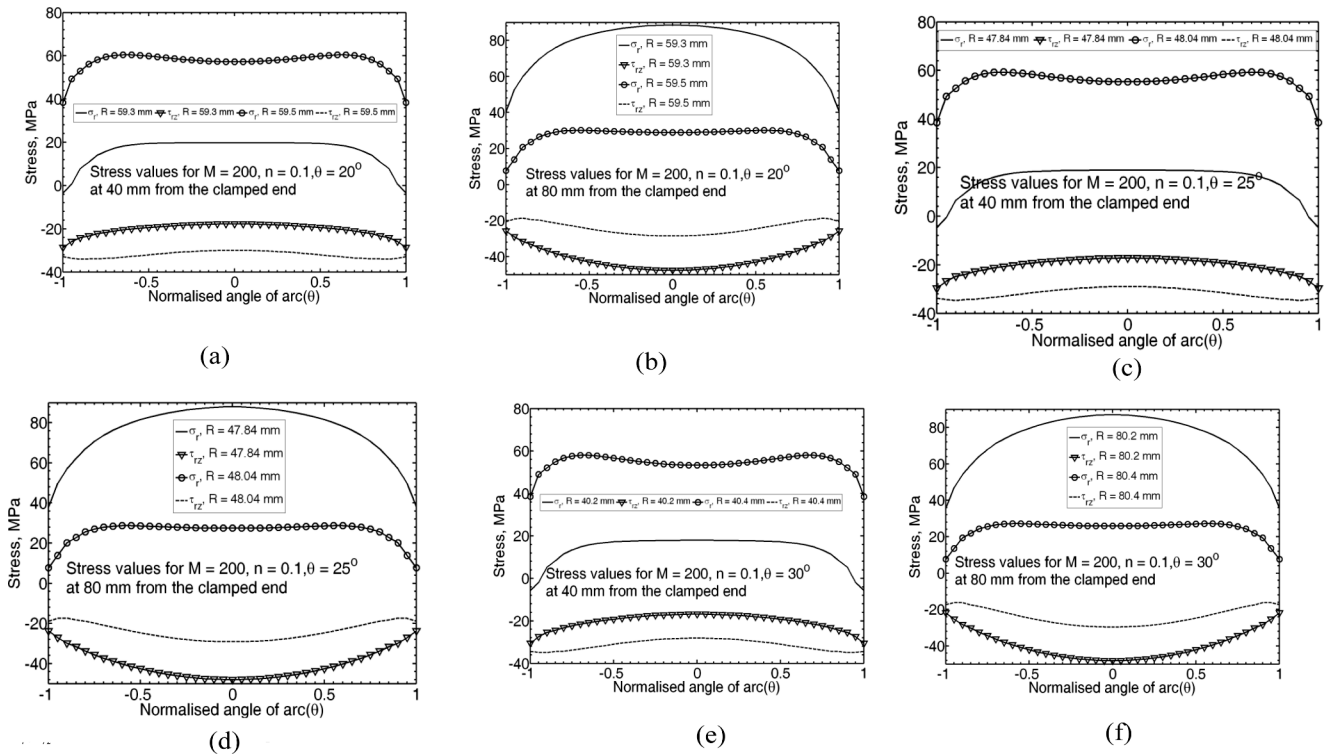


Fig. 5 Variations of stress (σ_r, τ_{rz}) along the angle of arcs with respect to $\theta = 20^\circ, 25^\circ, 30^\circ$ panels at 40 mm and 80 mm from the clamped end. (a) Stresses (σ_r, τ_{rz}) for $\theta = 20^\circ$ at 40 mm form clamped end. (b) Stresses (σ_r, τ_{rz}) for $\theta = 20^\circ$ at 80 mm form clamped end. (c) Stresses (σ_r, τ_{rz}) for $\theta = 25^\circ$ at 40 mm form clamped end. (d) Stresses (σ_r, τ_{rz}) for $\theta = 25^\circ$ at 80 mm form clamped end. (e) Stresses (σ_r, τ_{rz}) for $\theta = 30^\circ$ at 40 mm form clamped end. (f) Stresses (σ_r, τ_{rz}) for $\theta = 30^\circ$ at 80 mm form clamped end $R = 40.2$ and 40.4 mm

Fig. 6 Variations of SERR with adhesion failure sizes for different compositional gradient exponent (n). (a) G_I variation for all n . (b) G_{II} variation for all n . (c) G_T variation for all n

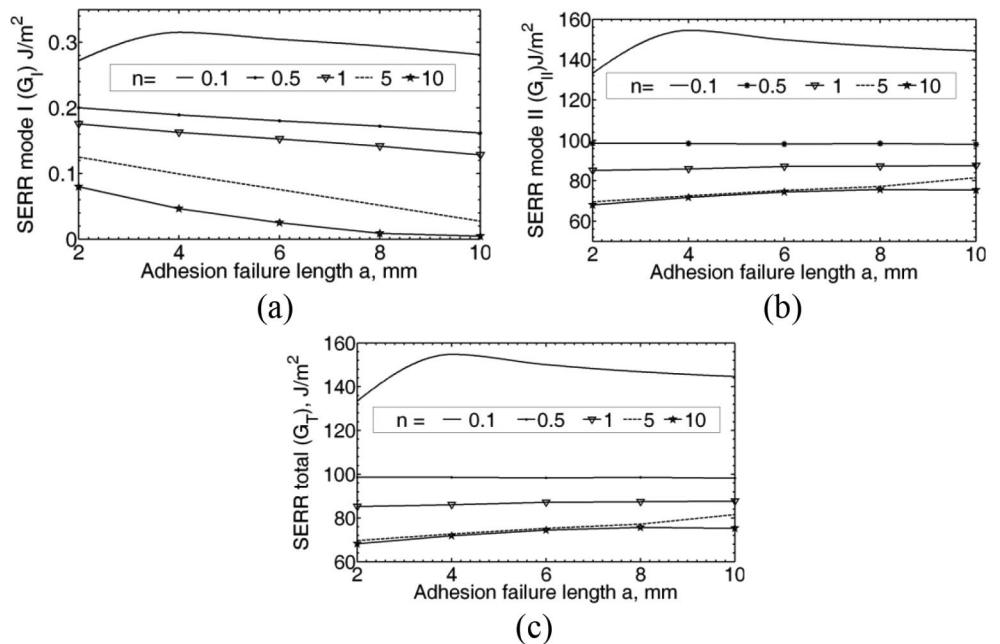
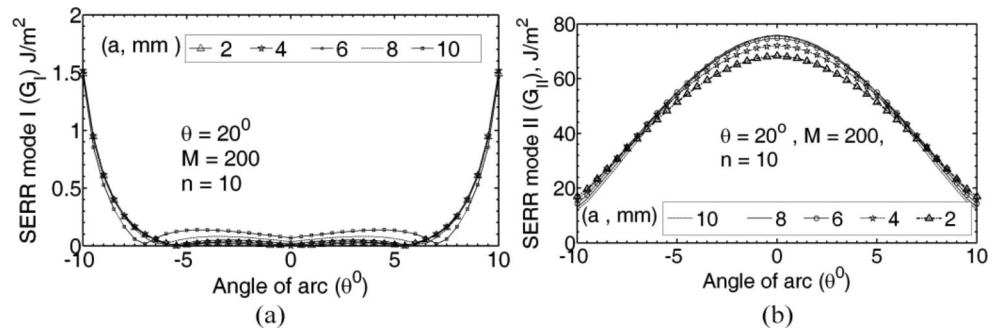


Figure 7(a) shows the variation of SERR (G_I) in the opening mode of adhesion failure propagation, and Fig. 7 (b) shows the variation of SERR (G_{II}) in the sliding mode of adhesion failure propagation through the width of

the panel. The sliding mode of failure propagation is the dominating mode of failure, and it is maximum at the central location, whereas the opening mode of failure starts from the edges of the panel.

Fig. 7 (a) Variations of SERR mode I (G_I) with adhesion failure sizes along the circumferential width for $\theta = 20^\circ$. (b) Variations of SERR mode II (G_{II}) with adhesion failure sizes along the circumferential width for $\theta = 20^\circ$



- The above discussions show that adhesion failure propagates in a mixed mode manner being dominated by sliding mode (G_{II}). The cross-sliding mode Further, the uneven variations G_I, G_{II} indicate a non-self-similar propagation adhesion failure front. The values of G_T (Fig. 6 (c)) increase with the increase in the size of the adhesion failure for all values n . It is also seen that the magnitude of total SERR (G_T) increases with adhesion failure size for smaller adhesion failure lengths ($a = 2$ to 5) in case of adherends having compositional gradient exponent $n = 1$, and for higher adhesion failure lengths, the magnitude G_T decreases with an increase in adhesion failure size. From Fig. 7(c), the adhesion failure will grow slower for adherend material with exponent $n = 10$ and best among all values of n . Also, the peel and shear stress values decreased slightly for the angle of the arc $\theta = 25^\circ, 30^\circ$ compared to the overlap ends of SLJ, as shown in Fig. 5.

4 Summary and conclusions

Functionally graded materials of the adherends improved the performance of the joint by redistributing the stresses in the critical locations of the SLJ. The gradual change of the property of the material as per the power law variation optimises the performance by exhibiting better damage tolerance because of their continuous variation of properties. It reduces the strain energy release rate, a quantifying parameter for adhesion failure growth assessment. This is particularly useful for green composites; otherwise, the adherends would have a weaker interface for fibre-epoxy composite laminates, which can have a matrix cracking or fibre breakage. It reduces resource consumption as bonding between natural fibre and matrix is one of the challenges in the green composite. FGM helps improve the adhesion and load transfer mechanism by influencing the differential straining and bending due to the eccentric load transfer path. Hence, it can be tailor-made for specific applications. This research guides designing a single lap joint with the proper

functional grading scheme to make a joint more efficient and eco-friendly, particularly for the marine and aerospace industry. FGMs can be engineered for specific applications by varying the composition and structure of the material. This level of customisation can be challenging to achieve with FRP composites. Three-dimensional non-linear finite element analyses have been carried out for pre-existing adhesion failure propagation in adhesively bonded SLJs made with curved FGM panels. The effect of different sizes of embedded adhesion failure lengths on the peel and shear stresses at adhesive and adherend interfaces have been studied in detail. The SERRs have been evaluated for varying adhesion failure lengths. The salient observations are as follows:

- The variation of failure prompting stresses demonstrates the existence of three three-dimensional stress states in the vicinity of the adhesion failure region. Hence, a 3-D analysis of the adhesively bonded curved adherends is required.
- The magnitudes and nature of inter-laminar stresses at the edge of the curved panels and the central portion of adherends used in SLJ are significantly different, indicating a severe edge effect. This further emphasises the requirement of adopting 3-D FE analyses to reduce the chance of errors creeping in by the 2-D analyses.
- The effect of curvature geometry on stresses in the adhesive-adherend interface of SLJ made with FGM adherend panel is not much.
- The SERR component G_I for the adhesion failure front is lower than G_{II} .
- The uneven variations of $G_T = G_I + G_{II}$ Demonstrates a mixed mode propagation with a non-self-similar adhesion failure front propagation.
- Based on the values of G_T compositional gradient, the exponent of functionally graded curved adherend $n = 10$ should be chosen for a lower rate of growth of adhesion failure.

Funding Not applicable.

Declarations

Conflicts of interest/Competing interests The authors certify that they have NO affiliations with or involvement in any organisation or entity with any financial interest (such as honoraria; educational grants; participation in speakers' bureaus; membership, employment, consultancies, stock ownership, or other equity interest; and expert testimony or patent-licensing arrangements), or non-financial interest (such as personal or professional relationships, affiliations, knowledge or beliefs) in the subject matter or materials discussed in this manuscript. This statement is agreed by all the authors to indicate agreement that the above information is true and correct.

References

- Volkersen, O.: Die nietkraftverteilung in zugbeanspruchten mit konstanten laschenquerschritten. *Luftfahrtforschung*. **15**, 7–41 (1938)
- Banea M.D., Da Silva L.F.M.: Adhesively bonded joints in composite materials: An overview. *Proc. Inst. Mech. Eng. Part. L J. Mater. Des. Appl.* **223**(1), 1–18 (2009). <https://doi.org/10.1243/14644207JMDA219>
- Wang, S.S., Yau, J.F.: Interface cracks in adhesively bounded lap-shear joints. *Int. J. Fract.* **19**(4), 295–309 (1982). <https://doi.org/10.1007/BF00012485>
- Tong, L.: 1988; Chai, 1988; Fernlund. *Science* (80-), no. 1944 (1998).
- Tay, T.E.: Characterisation and analysis of delamination fracture in composites: An overview of developments from 1990 to 2001. *Appl. Mech. Rev.* **56**(1), 1–31 (2003). <https://doi.org/10.1115/1.1504848>
- Carpenter, W.C.: A comparison of numerous lap Joint theories for Adhesively Bonded joints. *J. Adhes.* **35**(1), 55–73 (1991). <https://doi.org/10.1080/00218469108030435>
- Wang, J.T., Raju, I.S.: Strain energy release rate formulae for skin-stiffener debond modeled with plate elements. *Eng. Fract. Mech.* **54**(2), 211–228 (1996). [https://doi.org/10.1016/0013-7944\(95\)00088-7](https://doi.org/10.1016/0013-7944(95)00088-7)
- Cheuk, P.T., Tong, L.: Failure of adhesive bonded composite lap shear joints with embedded precrack. *Compos. Sci. Technol.* **62**(7–8), 1079–1095 (2002). [https://doi.org/10.1016/S0266-3538\(02\)00054-4](https://doi.org/10.1016/S0266-3538(02)00054-4)
- Edde, F., Verreman, Y.: On the fracture parameters in a clamped cracked lap shear adhesive joint. *Int. J. Adhes. Adhes.* **12**(1), 43–48 (1992). [https://doi.org/10.1016/0143-7496\(92\)90007-1](https://doi.org/10.1016/0143-7496(92)90007-1)
- Lai, Y.H., Rakestraw, M.D., Dillard, D.A.: The cracked lap shear specimen revisited - a closed form solution. *Int. J. Solids Struct.* **33**(12), 1725–1743 (1996). [https://doi.org/10.1016/0020-7683\(95\)00124-7](https://doi.org/10.1016/0020-7683(95)00124-7)
- Apalak, M.K., Gunes, R., Eroglu, S.: Thermal residual stresses in an adhesively bonded functionally graded tubular single lap joint. *Int. J. Adhes. Adhes.* **27**(1), 26–48 (2007). <https://doi.org/10.1016/j.ijadhadh.2005.09.009>
- Kumar, S.: Analysis of tubular adhesive joints with a functionally modulus graded bondline subjected to axial loads. *Int. J. Adhes. Adhes.* **29**(8), 785–795 (2009). <https://doi.org/10.1016/j.ijadhadh.2009.06.006>
- Reddy, J.N.: Analysis of functionally graded plates. *Int. J. Numer. Methods Eng.* **47**(1–3), 663–684 (2000). [https://doi.org/10.1002/\(SICI\)1097-0207\(20000110/30\)47:1/3<663::AID-NME787>3.0.CO;2-8](https://doi.org/10.1002/(SICI)1097-0207(20000110/30)47:1/3<663::AID-NME787>3.0.CO;2-8)
- Rybicki, E.F., Kanninen, M.F.: A finite element calculation of stress intensity factors by a modified crack closure integral. *Eng. Fract. Mech.* **9**(4), 931–938 (1977). [https://doi.org/10.1016/0013-7944\(77\)90013-3](https://doi.org/10.1016/0013-7944(77)90013-3)
- Cengiz, G.D., Mehmet, D.: A unified phase-field approach for failure prediction in modulus graded adhesively bonded single-lap joints. *Theoretical App Frac Mech.* **127**, 104062 (2023). <https://doi.org/10.1016/j.tafmec.2023.104062>
- Mehdi, V., Arash, R., Younes, S.: Stress analysis of adhesively-bonded single stepped-lap joints with functionally graded adherends based on the four-parameter fractional viscoelastic model. *Eur. J. Mech. A. Solids.* **98**, 104907 (2023). <https://doi.org/10.1016/j.euromechsol.2022.104907>
- Khan, M.A., Tipireddy, R., Dattaguru, B., Kumar, S.: Stochastic modelling of functionally graded double lap adhesive joints. *Mech. Mater.* **177** (2023). <https://doi.org/10.1016/j.mechmat.2022.104553>
- Koizumi, M.: FGM activities in Japan. *Compos. Part. B-engineering.* **28**, 1–4 (1997)
- Kim, M.H., Ri, J.H., Hong, H.S.: A 3-D numerical modeling for prediction of mixed failure characteristics in composite single lap joints with hybrid adhesive layer. *Int. J. Adhes. Adhes.* **118**, 103223 (2022). <https://doi.org/10.1016/j.ijadhadh.2022.103223>
- Behera, R., Parida, S.K., Das, R.R.: Effect of pre-embedded adhesion failures and surface ply delaminations on the structural integrity of adhesively bonded single lap joints made with curved laminated FRP composite panels. *Int. J. Adhes. Adhes.* **108**, 102887 (2021). <https://doi.org/10.1016/j.ijadhadh.2021.102887>
- Parida, S.K., Pradhan, A.K.: 3D FE delamination induced damage analyses of adhesive bonded lap shear joints made with curved laminated FRP composite panels. *J. Adhes. Sci. Technol.* **27**(10), 1104–1121 (2013). <https://doi.org/10.1080/01694243.2012.733670>

Publisher's Note Springer Nature remains neutral with regard to jurisdictional claims in published maps and institutional affiliations.

Springer Nature or its licensor (e.g. a society or other partner) holds exclusive rights to this article under a publishing agreement with the author(s) or other rightsholder(s); author self-archiving of the accepted manuscript version of this article is solely governed by the terms of such publishing agreement and applicable law.